

SEARCHING FOR UNSEEN PLANETS VIA OCCULTATION AND MICROLENSING

PENNY D. SACKETT
Kapteyn Astronomical Institute
Postbus 800, 9700 AV Groningen, The Netherlands
psackett@astro.rug.nl

Abstract.

The fields of occultation and microlensing are linked historically. Early this century, occultation of the Sun by the Moon allowed the apparent positions of background stars projected near the limb of the Sun to be measured and compared with their positions six months later when the Sun no longer influenced the light path to Earth. The measured shift in the stellar positions was consistent with lensing by the gravitational field of the Sun during the occultation, as predicted by the theory of general relativity. This series of lectures explores the principles, possibilities and challenges associated with using occultation and microlensing to discover and characterize unseen planets orbiting distant stars. The two techniques are complementary in terms of the information that they provide about planetary systems and the range of system parameters to which they are most sensitive. Although the challenges are large, both microlensing and occultation may provide avenues for the discovery of extra-solar planets as small as Earth.

1. Introduction

Indirect methods to search for extra-solar planets do not measure emission from the planet itself, but instead seek to discover and quantify the tell-tale effects that the planet would have on the position (astrometry) and motion (radial velocity) of its parent star, or on the apparent brightness of its parent star (occultation) or random background sources (gravitational microlensing). All of these indirect signals have a characteristic temporal behavior that aids in the discrimination between planetary effects and other

astrophysical causes. The variability can be due to the changing position of the planet with respect to the parent star (astrometry, radial velocity, occultation), or the changing position of the complete planetary system with respect to background stars (microlensing). The time-variable photometric signals that can be measured using occultation and microlensing techniques are the focus of this small series of lectures.

An occultation is the temporary dimming of the apparent brightness of a parent star that occurs when a planet transits the stellar disk; this can occur only when the orbital plane is nearly perpendicular to the plane of the sky. Because the planet is considerably cooler than its parent star, its surface brightness at optical and infrared wavelengths is less, causing a dip in the stellar light curve whenever the planet (partially) eclipses the star. Since the fractional change in brightness is proportional to the fraction of the stellar surface subtended by the planetary disk, photometric measurements directly yield a measure of the planet's size. For small terrestrial planets, the effect is simply to occult a fraction of the stellar light; the atmospheres of larger gaseous planets may also cause absorption features that can be measured during transit with high resolution, very high S/N spectroscopic monitoring.

The duration of a transit is a function of the size of the stellar disk and the size and inclination of the planetary orbit. Together with an accurate stellar typing of the parent star, measurement of the transit duration and period provides an estimate for the radius and inclination of the planet's orbital plane. Since large planets in tight orbits will create the most significant and frequent occultations, these are the easiest to detect. If hundreds of stars can be monitored with significantly better than 1% photometry, the transit method can be applied from the ground to place statistics on Jupiter-mass planets in tight orbits. Space-based missions, which could search for transits continuously and with higher photometric precision, may be capable of detecting Earth-mass planets in Earth-like environments via the occultation method. Moons or multiple planets may also be detectable, not through their eclipsing effect, but by the periodic change they induce in the timing of successive transits of the primary occulting body.

Microlensing occurs when a foreground compact object (e.g., a star, perhaps with orbiting planets) moves between an observer and a luminous background source (e.g., another star). The gravitational field of the foreground lens alters the path of the light from the background source, creating multiple images with a combined brightness larger than that of the unlensed background source. For stellar or planetary mass lenses, the separation of these images is too small to be resolved, but the combined brightness of the images changes with time in a predictable manner as the lensing system moves across the sky with respect to the background source.

Hundreds of microlensing events have been detected in the Galaxy, a large fraction of which are due to (unseen) stellar lenses. In binary lenses with favorable geometric configurations, the lensing effect of the two lenses combines in a non-linear way to create detectable and rapid variations in the light curve of the background source star. Modeling of these features yields estimates for the mass ratio and normalized projected orbital radius for the binary lens; in general, smaller-mass companions produce weaker and shorter deviations.

Frequent, high-precision photometric monitoring of microlensing events can thus be used to discover and characterize extreme mass-ratio binaries (i.e., planetary systems). With current ground-based technology, microlensing is particularly suited to the detection of Jupiter-mass planets in Jupiter-like environments. Planets smaller than Neptune will resolve the brightest background sources (giants) diluting the planetary signal. For planets above this mass, the planetary detection efficiency of microlensing is a weak function of the planet's mass and includes a rather broad range in orbital radii, making it one of the best techniques for a statistical study of the frequency and nature of planetary systems in the Galaxy. Microlensing can discover planetary systems at distances of the Galactic center and is the only technique that is capable of detecting unseen planets around *unseen parent stars!*

These lectures begin with a discussion of the physical basis of occultation and microlensing, emphasizing their strengths and weaknesses as well as the selection effects and challenges presented by sources of confusion for the planetary signal. The techniques are then placed in the larger context of extra-solar planet detection. Speculative comments about possibilities in the next decade cap the lectures.

2. Principles of Planet Detection via Occultations

Due to their small sizes and low effective temperatures, planets are difficult to detect directly. Compared to stars, their luminosities are reduced by the square of the ratio of their radii (factors of $\sim 10^{-2} - 10^{-6}$ in the Solar System) and the fourth power of the ratio of their effective temperatures (factors of $\sim 10^{-4} - 10^{-9}$ in the Solar System). Such planets may be detected indirectly however if they chance to transit (as viewed by the observer) the face of their parent star and are large enough to occult a sufficient fraction of the star's flux. This method of detecting planets around other stars was discussed as early as mid-century (Sturve 1952), but received serious attention only after the detailed quantification of its possibilities by Rosenblatt (1971) and Borucki and Summers (1984).

Such occultation effects have been observed for many years in the pho-

tometry of binary star systems whose orbital planes lie close enough to edge-on as viewed from Earth that the disk of each partner occults the other at some point during the orbit, creating two dips in the combined light curve of the system. The depth of the observed occultation depends on the relative size and temperatures of the stars. For planetary systems, only the dip caused by the occultation of the brighter parent star by the transit of the smaller, cooler planet will be detectable. The detection rate for a given planetary system will depend on several factors: the geometric probability that a transit will occur, the frequency and duration of the observations compared to the frequency and duration of the transit, and the sensitivity of the photometric measurements compared to the fractional deviation in the apparent magnitude of the parent star due to the planetary occultation. We consider each of these in turn.

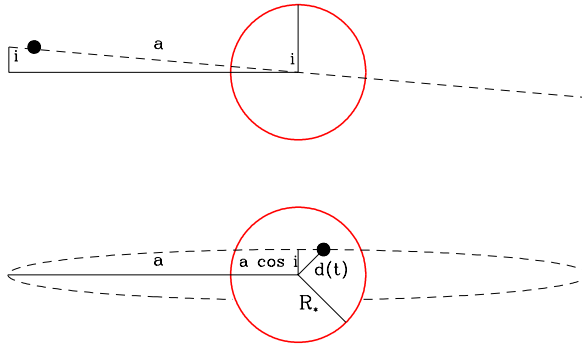


Fig. 1 — Geometry of a transit event of inclination i and orbital radius a as seen from the side (top) and observer’s vantage point (bottom) at a moment when the planet lies a projected distance $d(t)$ from the stellar center.

Unless stated otherwise in special cases below, we will assume for the purposes of discussion that planetary orbits are circular and that the surface brightness, mass, and radius of the planet are small compared to that of the parent star. We will also assume that the orbital radius is much larger than the size of the parent star itself.

2.1. GEOMETRIC PROBABILITY OF A TRANSIT

Consider a planet of radius R_p orbiting a star of radius R_* and mass M_* at an orbital radius a . A transit of the stellar disk will be seen by an external observer only if the orbital plane is sufficiently inclined with respect to the sky plane (Fig. 1). In particular, the inclination i must satisfy

$$a \cos i \leq R_* + R_p \quad . \quad (1)$$

Since $\cos i$ is simply the projection of the normal vector (of the orbital plane) onto the sky plane, it is equally likely to take on any random value between 0 and 1. Thus, for an ensemble of planetary systems with arbitrary orientation with respect to the observer, the probability that the inclination satisfies the geometric criterion for a transit is:

$$\text{Geometric Transit Prob} = \frac{\int_0^{(R_*+R_p)/a} d(\cos i)}{\int_0^1 d(\cos i)} = \frac{R_* + R_p}{a} \approx \frac{R_*}{a} \quad (2)$$

Geometrically speaking, the occultation method favors those planets with small orbital radii in systems with large parent stars. As can be seen in Fig. 2, for planetary systems like the Solar System this probability is small: $\lesssim 1\%$ for inner terrestrial planets and about a factor of 10 smaller for jovian gas giants. This means that unless a method can be found to pre-select stars with ecliptic planes oriented perpendicular to the plane of the sky, thousands of random stars must be monitored in order to detect statistically meaningful numbers of planetary transits due to solar systems like our own.

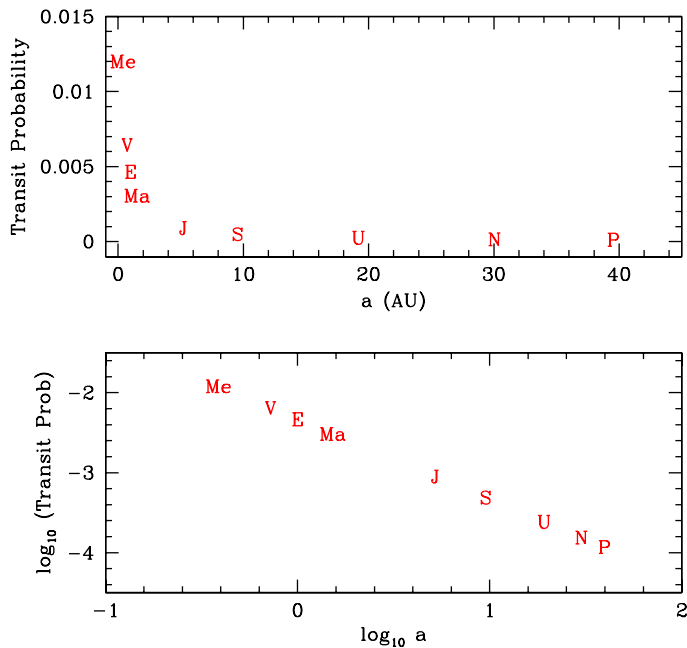


Fig. 2 — Probability of transits by Solar System objects as seen by a random external observer.

2.1.1. Inclination Pre-selection

Under the assumption that the orbital angular momentum vector of a planetary system and the rotational angular momentum vector of the parent star share a common origin and thus a common direction, single stars can be pre-selected for transit monitoring programs on the basis of a measurement of their rotational spin. In this way, one may hope to increase the chances of viewing the planetary orbits edge-on. Through spectroscopy, the line-of-sight component of the rotational velocity $v_{*,los}$ of a star's atmosphere can be measured. The period $P_{*,rot}$ of the rotation can be estimated by measuring the periodic photometric signals caused by sunspots, and the radius R_* of the star can be determined through spectral typing and stellar models. An estimate for the inclination of the stellar rotation plane to the plane of the sky can then be made:

$$\sin i_{*,rot} = \frac{v_{*,los} P_{*,rot}}{2\pi R_*} \quad , \quad (3)$$

and only those stars with high rotational inclinations selected to be monitored for transits.

How much are the probabilities increased by such pre-selection? Fig. 3 shows the probability of the planetary orbital inclination being larger (more edge-on) than a particular value ranging from $89.5^\circ < i < 85^\circ$, if the parent star is pre-selected to have a rotational plane with inclination $i_{*,rot} \geq i_{select}$.

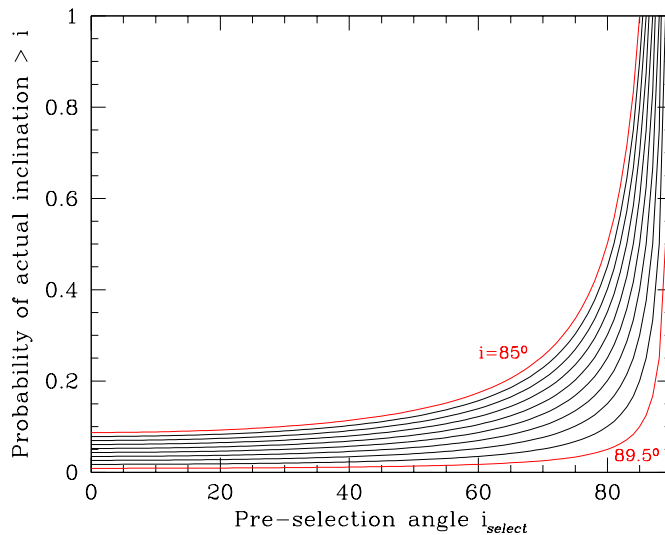


Fig. 3 — Increase of geometric transit probability through pre-selection of the inclination angle to be larger than i_{select} , for example through measurement of the rotational spin of the parent.

In order to produce a detectable transit, most planets will require an orbital inclination $\lesssim 1^\circ$ from edge-on. If planetary systems could be pre-selected to have $i > 85$, the geometric transit probability would be increased by a factor of ~ 10 . Unfortunately, measurement uncertainties in the quantities required to determine $\sin i_{*,rot}$ are likely to remove much of the advantage that pre-selection would otherwise afford. Since $\delta(\cos i) = -\tan i \delta(\sin i)$, even small errors in $\sin i_{*,rot}$ translate into large uncertainties in $\cos i_{*,rot}$ and thus the probability that a transit will occur. Furthermore, an accurate measurement of $\cos i_{*,rot}$ does not ensure that $\cos i$ for the planetary orbital plane is known. The planets in our own Solar System are misaligned by about 7° with the Sun's rotational plane, a result that is similar to that found for binaries orbiting solar-type stars (Hale 1994). It is thus reasonable to assume that an accurate measurement of $i_{*,rot}$ will constrain the planetary orbital plane only to within $\sim 10^\circ$.

To enhance probabilities, current ground-based attempts to detect transits have taken a different tack by concentrating on known eclipsing binary star systems in which the orbital plane of the binary is known to be close to edge-on. Assuming that any other companions will have similarly aligned angular momentum vectors, it is hoped that such systems will have larger than random chances of producing a transit event. The precession of orbital plane likely to be present in such systems may actually bring the planet across the face of the star more often than in single star systems (Schneider 1994). On the other hand, the evolution and dynamics of single and double star systems is so different that the formation and frequency of their planetary companions is likely to be quite different as well. In particular, it may be difficult for planets in some binary systems to maintain long-lived circular orbits and thus, perhaps, to become the birth place of life of the sort that has evolved on Earth.

Given the uncertainties involved, inclination pre-selection in single stars is unlikely to increase geometric transit probabilities by factors larger than 3 – 5. Ambitious ground-based and space-based initiatives, however, may monitor so many stars that pre-selection is not necessary.

2.2. TRANSIT DURATION

The duration and frequency of the expected transits will determine the observational strategy of an occultation program. The frequency is simply equal to one over the orbital period $P = \sqrt{4\pi^2 a^3 / GM_*}$. If two or more transits for a given system can be measured and confirmed to be due to the same planet, the period P and orbital radius a are determined. In principle, the ratio of the transit duration to the total duration can then be used to determine the inclination of the orbital plane, if the stellar radius is known.

The duration of the transit will be equal to the fraction of the orbital period P during which the projected distance d between the centers of the star and planet is less than the sum of their radii $R_* + R_p$. Referring to Fig. 4 we have

$$\text{Duration} \equiv t_T = \frac{2P}{2\pi} \arcsin \left(\frac{\sqrt{(R_* + R_p)^2 - a^2 \cos^2 i}}{a} \right) , \quad (4)$$

which for $a \gg R_* \gg R_p$ becomes

$$t_T = \frac{P}{\pi} \sqrt{\left(\frac{R_*}{a}\right)^2 - \cos^2 i} \leq \frac{P R_*}{\pi a} . \quad (5)$$

Note that because the definition of a transit requires that $a \cos i \leq (R_* + R_p)$, the quantity under the square root in Eq. 4 does not become negative.

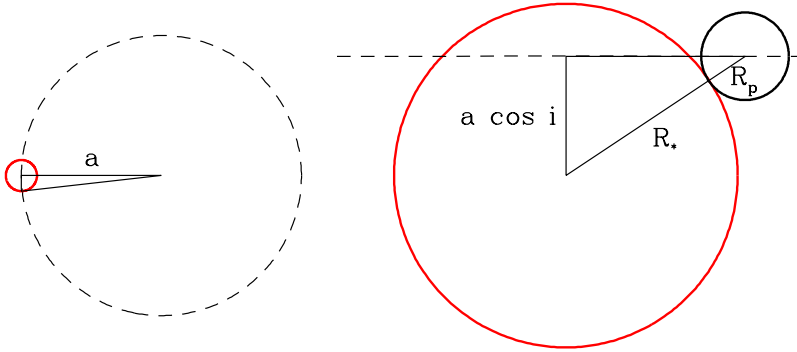


Fig. 4 — Transit duration is set by fraction of total orbit (left) for which a portion of the planet eclipses the stellar disk (right).

Fig. 5 shows the maximum transit duration and period for planets in the Solar System. In order to confirm a planetary detection with one or more additional transits after the discovery of the first eclipse, a 5-year experiment can be sensitive to planets orbiting solar-type stars only if their orbital radius is equal to or smaller than that of Mars. Such planets will have transit durations of less than one day, requiring rapid and continuous sampling to ensure high detection probabilities.

The actual transit duration depends sensitively on the inclination of the planetary orbit with respect to the observer, as shown in Fig. 6. The transit time of Earth as seen by an external observer changes from 0.5 days to zero (no transit) if the observers viewing angle is more than 0.3° from optimal. Since the orbital planes of any two of the inner terrestrial planets in the

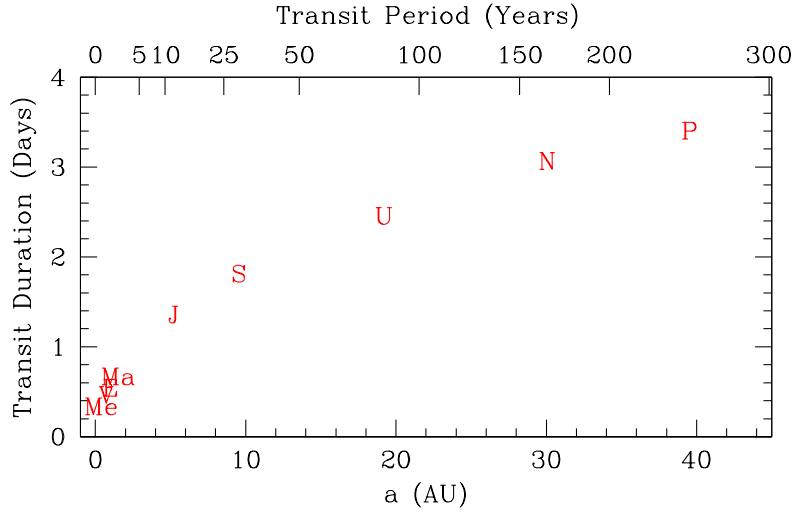


Fig. 5 — Edge-on transit durations and periods for Solar System planets.

Solar System are misaligned by 1.5° or more, if other planetary systems are like our own, a given observer would expect to see transits from only one of the inner planets. This would decrease the detection probabilities for planetary systems, but also the decrease the probability of incorrectly attributing transits from different planets to successive transits of one (mythical) shorter period object.

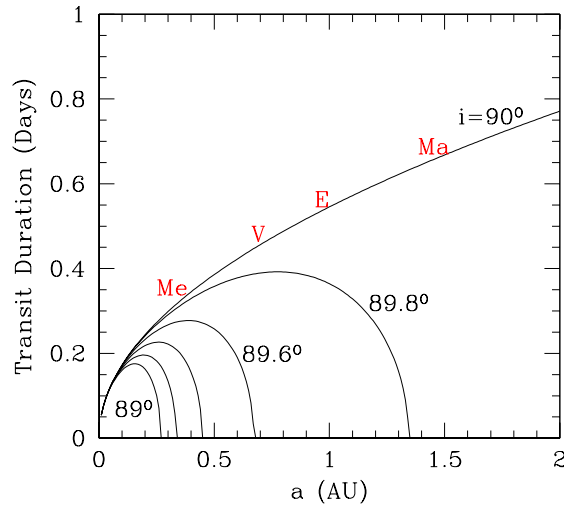


Fig. 6 — “Inner planet” transit durations for different inclinations ($R_* = R_\odot$).

If the parent star can be typed spectroscopically, stellar models can provide an estimate for the stellar radius R_* in the waveband in which

the photometric partial eclipse was measured. (It is important to match wavebands since limb-darkening can make the star look larger at redder wavelengths which are more sensitive to the cooler outer atmosphere of the star.) The temporal resolution of a single transit then places a lower limit on the orbital radius a of the planet, but a full determination of a requires knowledge of the period from multiple transit timings which remove the degeneracy due to the otherwise unknown orbital inclination. In principle, if the limb darkening of the parent star is sufficiently well-understood, measurements in multiple wavebands can allow an estimate for the inclination, and thus for a from a single transit; this is discussed more fully in §2.3.1.

2.3. AMPLITUDE AND SHAPE OF THE PHOTOMETRIC SIGNATURE

Planets with orbital radii of 2 AU or less orbiting stars even as close as 10 parsec will subtend angles $\lesssim 50$ microarcseconds; any reflected or thermal radiation that they might emit thus will be confused by normal photometric techniques with that from the parent star. Only exceedingly large and close companions of high albedo would be capable of creating a significant modulated signal throughout their orbit as the viewer sees a different fraction of the starlit side; we will not consider such planets here. All other planets will alter the total observed flux only during an actual transit of the stellar face, during which the amplitude and shape of the photometric dip will be determined by the fraction of the stellar light that is occulted as a function of time.

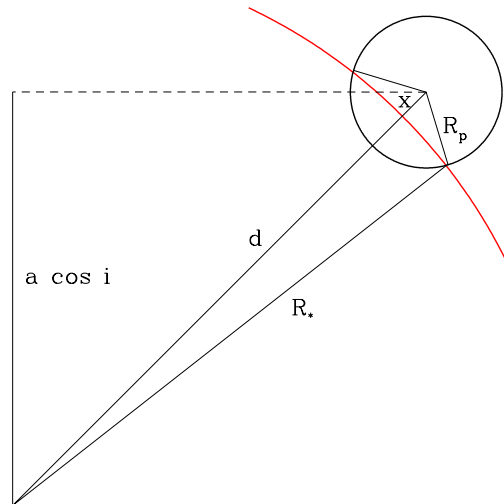


Fig. 7 — The area eclipsed by a planet as it crosses the stellar limb determines the wing shape of the resulting photometric dip.

The maximum fractional change in the observed flux is given by:

$$\text{Maximum } \frac{|\delta\mathcal{F}_\lambda|}{\mathcal{F}_\lambda} = \frac{\pi\mathcal{F}_{\lambda,*} R_p^2}{\pi\mathcal{F}_{\lambda,*} R_*^2 + \pi\mathcal{F}_{\lambda,p} R_p^2} \approx \left(\frac{R_p}{R_*}\right)^2 \equiv \rho^2 \quad (6)$$

The shape of the transit dip will depend on the inclination angle, the ratio of the planet to stellar size, and the degree of limb-darkening in the observational band.

Begin by considering a star of uniform brightness (no limb-darkening) transited by a small planet. The stellar limb will then describe a nearly straight chord across the planet at any time, and integration over planet-centered axial coordinates (see Fig. 7) yields an eclipsing area during ingress and egress of:

$$\mathcal{A}_\mathcal{E} \approx \int_x^{R_p} r_p dr_p \int_{-\arccos(x/r_p)}^{+\arccos(x/r_p)} d\phi_p = 2 \int_x^{R_p} r_p \arccos\left(\frac{x}{r_p}\right) dr_p \quad , \quad (7)$$

where $x \equiv d - R_*$, d is the projected star-planet separation and x is constrained to lie in the region $-R_p < x < R_p$. The last integral can be done analytically to yield,

$$\mathcal{A}_\mathcal{E} \approx R_p^2 \arccos(x/R_p) - R_p x \sqrt{1 - \frac{x^2}{R_p^2}} \quad . \quad (8)$$

For larger planets, and to facilitate the introduction of limb-darkened sources, it is more useful to integrate over stellar-centered axial coordinates; the Law of Cosines can then be used to show that

$$\mathcal{A}_\mathcal{E}(t) = 2 \int_{\max(0, d(t)-R_p)}^{\min(R_*, d(t)+R_p)} r_* \arccos[\Theta(t)] dr_* \quad (9)$$

$$\text{where } \Theta(t) \equiv \frac{d^2(t) + r_*^2 - R_p^2}{2r_*d(t)} \quad \text{for } r_* > R_p + d(t), \text{ and } \pi \text{ otherwise.} \quad (10)$$

The light curve resulting from the occultation of a uniform brightness source by a planet of arbitrary size, orbital radius and orbital inclination can now be constructed by substituting into Eq. 9 the time dependence of the projected planet-star separation, $d(t) = a \sqrt{\sin^2 \omega t + \cos^2 i \cos^2 \omega t}$, where $\omega \equiv 2\pi/P$. The *differential* light curve is then given by:

$$\frac{\mathcal{F}(t)}{\mathcal{F}_0} = 1 - \frac{\mathcal{A}_\mathcal{E}(t)}{\pi R_*^2} \quad (11)$$

For spherical stars and planets, the light curve will be symmetric and have a minimum at the closest projected approach of planet to star center, where the fractional decrease in the total brightness will be less than or equal to $(R_p/R_*)^2$. For Jupiter-sized planets orbiting solar-type stars, this is a signal of $\sim 1\%$; for Earth-sized planets the fractional change is $\lesssim 0.01\%$ (Fig. 8).

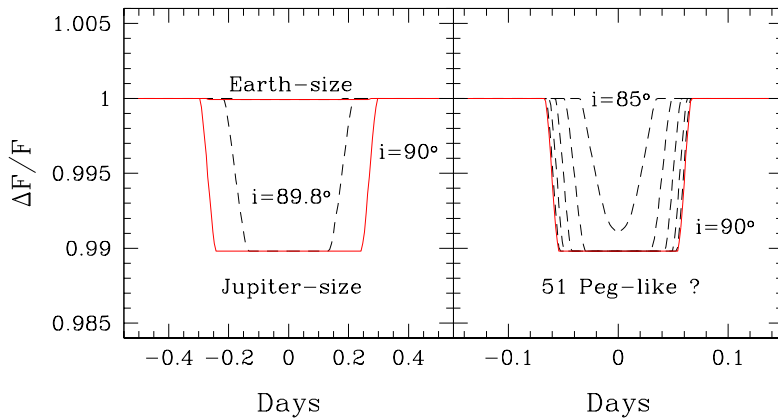


Fig. 8 — **Left:** Photometric light curves for Earth-sized and Jupiter-sized planets orbiting a solar-type star at 1 AU. **Right:** A Jupiter-sized planet orbiting a solar-type star at an orbital radius of 0.05 AU (e.g., 51 Peg) with inclinations ranging from 85° to 90° . The parent star is assumed here to have constant surface brightness. Note change in time scale between two panels.

If proper care is taken, photometry of bright, uncrowded stars can be performed to $\sim 0.1\%$ precision from the ground (Henry *et al.* 1997), so that ground-based transit searches can in principle be sensitive to Jupiter-sized planets at $\lesssim 1$ AU — planets perhaps similar to those being found by the radial velocity technique (e.g., Mayor & Queloz 1995, Butler & Marcy 1996). Transit detections of terrestrial planets like those in our own Solar System must await space observations in order to achieve the required photometric precision.

2.3.1. Effects of Limb Darkening

Because observations at different wavelengths probe material at different depths in stellar atmospheres, a stellar disk is differentially limb-darkened: the radial surface brightness profile $B_\lambda(r_*)$ of a star is wavelength dependent. In redder bands, which probe the cooler outer regions of the star, the stellar disk will appear larger and less limb-darkened. Limb darkening is important to transit techniques for two reasons: it changes the shape of the photometric signal and it does so in a wavelength-dependent way.

Since a given planet can produce dips of varying strength depending on the inclination i of the orbit, the inclination must be known in order to estimate the planet's radius R_p accurately. In principle, if the parent star has been typed so that its mass and stellar radius R_* are known, Kepler's Law together with Eq. 5 will yield i once the transit time t_T and period P have been measured. Ignoring the effects of limb darkening, however, will result in an underestimate of t_T , and thus an underestimate for the inclination i as well. In order to produce the required amplitude at minimum, the size of the planet R_p will then be overestimated. Furthermore, the sloping shape of the limb-darkened profile might be attributed to the smaller inclination i , reinforcing misinterpretation.

This difficulty will be removed if the limb darkening can be properly modeled. In addition, transit monitoring in more than one waveband could confirm the occultation hypothesis by measuring the characteristic color signature associated with limb darkening. In principle this signature can be used to determine the orbital inclination from a single transit, in which case Eq. 5 can be inverted to solve for the period P without waiting for a second transit.

How strong is the effect of limb darkening? To incorporate its effect, the integral in Eq. 9 used to determine the eclipsing area must be weighted by the surface brightness as a function of stellar radius, yielding the differential light curve:

$$\frac{\mathcal{F}_\lambda(t)}{\mathcal{F}_{\lambda,0}} = 1 - \frac{\int_{\max(0, d(t)-R_p)}^{\min(R_*, d(t)+R_p)} r_* B_\lambda(r_*) \arccos[\Theta(t)] dr_*}{\pi \int_0^{R_*} r_* B_\lambda(r_*) dr_*} \quad (12)$$

A commonly-used functional form for the surface brightness profile is $B_\lambda(\mu) = [1 - c_\lambda(1 - \mu)]$, where $\mu \equiv \cos \gamma$ and γ is the angle between the normal to the stellar surface and the line-of-sight. In terms of the projected radius r_* from the stellar center this can be written as $B_\lambda(r_*) = [1 - c_\lambda(1 - \sqrt{1 - (r_*/R_*)^2})]$. Using this form and constants c_λ appropriate for the Sun, light curves and color curves are shown in Fig. 9 for a Jupiter-sized planet orbiting 1 AU from a solar-type star at inclinations of 90° and 89.8° .

As expected, the bluer band shows more limb darkening, which rounds the sharp edges of the occultation profile making it qualitatively degenerate with a larger planet at somewhat smaller inclination. The color curves for different inclinations, however, are qualitatively different and can thus be used to break this degeneracy. During ingress and egress the color curve becomes bluer as the differentially redder limb is occulted; at maximum occultation the color curve is redder than the unocculted star for transits with inclination $i = 90^\circ$ since the relative blue central regions are then occulted. For smaller inclinations, the planet grazes the limb blocking preferentially

red light only, and the color curve stays blue through the event. Since the size of the color signal is $\sim 10\%$ of the deviation in total flux, excellent photometry is required to measure this effect and use it to estimate the orbital inclination; even for jovian giants it remains at or just beyond the current limits of photometric precision.

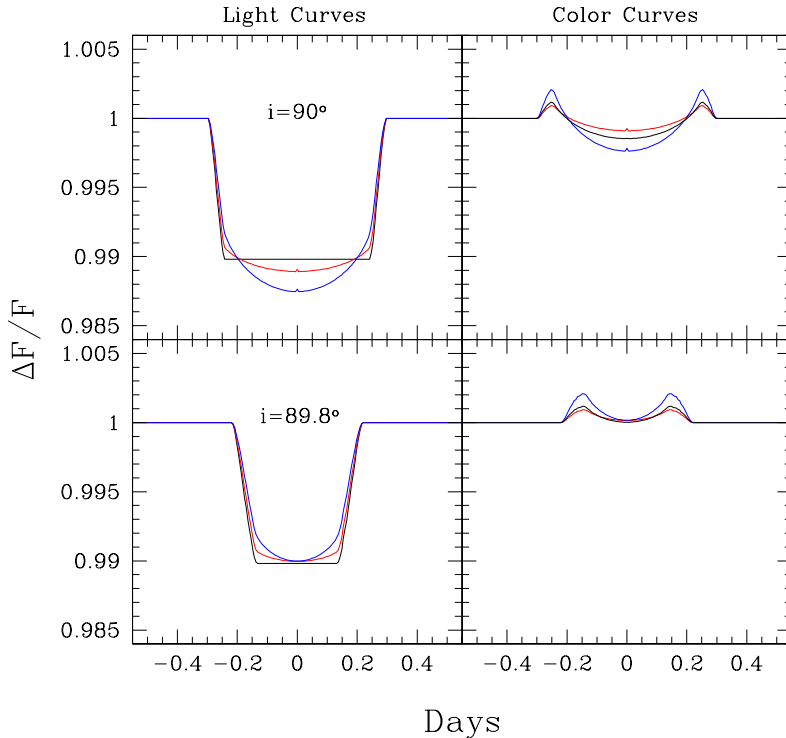


Fig. 9 — **Left:** Light curves for a planet with $R_p = 11R_\oplus$ orbiting a solar-type star with orbital inclinations of 90° (top) and 89.8° (bottom) normalized to the total (unocculted) flux in the indicated band. Black shows a uniformly bright stellar disk; blue and red indicate observations in the R and K bands respectively. **Right:** Color curves indicating the flux ratios at any given time between R (blue) and K-band (red) limb-darkened curves and a uniformly bright target star, and the observed limb-darkened R/K flux ratio (black).

2.4. OBSERVATIONAL REWARDS AND CHALLENGES

In sum, what can be learned by observing a planetary object transiting the face of its parent star? The amplitude of the photometric signal places a lower limit on the ratio of the planetary radius to stellar radius $\rho \equiv R_p/R_*$, while the duration of the event places a lower limit on the orbital period

P and thus on the orbital radius a as well. If the inclination i is known, these lower limits become measurements. In principle i could be determined by fitting the wings of the transit profile in different wavebands using the known limb-darkening of the star, but in practice this will probably prove too difficult. Instead, multiple transits will be required to time the transits and thus measure the period P of the planet, from which the inclination can be determined from the known transit duration (Eq. 5). This makes the transit method most appropriate for large planets orbiting their parent stars at (relatively) small radii a . The primary challenge then reduces to performing the very precise photometry required on a large enough sample of stars to place meaningful statistics on the numbers of planets at small a .

What limits the photometric accuracy and clear detection of a transit signal? The dwarf stars that have suitably small stellar radii R_* must have apparent magnitudes bright enough (ie, be close enough) that enough photons can be captured in short exposures so that a sub-day transit event can be well-sampled. This will limit the depth of the sample to only nearby stars. Fields with very high stellar densities (like globular clusters or the Galactic Center) or very wide fields that can capture hundreds of candidate stars simultaneously will be required in order to maintain the required temporal sampling on a large enough sample. Regions of high stellar density, however, will be hampered by the additional challenges associated with precision photometry in confused fields.

The use of reference constant stars in the field can reduce the effects of varying extinction to produce the best current photometry in uncrowded fields, precise to the $\sim 0.1\%$ level. Ultimately, scintillation, the rapidly-varying turbulent refocusing of rays passing through the atmosphere, limits Earth-bound photometry to 0.01% . Detection of Earth-mass transits is thus probably restricted to space-borne missions, although in special circumstances, periodicity analyses may be used to search for very short-period Earth-sized transits from the ground (e.g., Henry *et al.* 1997).

For larger, jovian gas-giants, the signal can be measured from the ground, but must be distinguished from intrinsic effects that could be confused with transits. Late-type dwarf stars often undergo pulsations that cause their brightness to vary on the order of a few hours, but due to their cyclic nature these pulsations should be distinguished easily from all but very short period transits corresponding to $a \lesssim 0.02$ AU or so.

Solar flares produce excess of flux at the $\lesssim 0.001\%$ level, and thus would not confuse a typical transit signal. Later-type dwarfs tend to have more surface activity, however, and thus produce flares that contain a larger fraction of the star's total flux. Since the flares are generally blue, the primary problem will be in confusing the chromatic signal expected due to limb-darkening effects during a transit.

More troublesome will be separating transits from irregular stellar variability due to star spots. Star spots are cool regions on the stellar surface that remain for a few rotations before disappearing. They could mock a transit event and thus are probably the most important non-instrumental source of noise. Although the power spectrum of the Solar flux does show variations on day and sub-day time scales, most of the power during periods of sunspot maximum occurs at the approximate 1-month time scale of the Sun's rotation. Even during sunspot maximum, variations on day and sub-day scales are at or below the 0.001% level (Borucki, Scargle & Hudson 1985). Star spots on solar-type stars will therefore not be confused with the transit signal of a gas giant, but spots might be a source of additional noise for terrestrial-sized planets of small orbital radius ($a \lesssim 0.3\text{AU}$) and for parent stars that are significantly more spotted than the Sun.

2.4.1. *Pushing the Limits: Rings, Moons and Multiple Planets*

If the parent star can be well-characterized, the transit method involves quite simple physical principles that can perhaps be exploited further to learn more about planetary systems. For example, if a system is discovered to contain large transiting inner planets, it can be assumed to have a favorable inclination angle that would make it a good target for more sensitive searches for smaller radius or larger a planets in the same system.

If the inner giants are large enough, differential spectroscopy with a very large telescope before and during transits could reveal additional spectral lines that could be attributed to absorption of stellar light by the atmosphere of the giant (presumably gaseous) planet (see Laurent & Schneider, this proceedings). A large occulting ring inclined to the observer's line-of-sight would create a transit profile of a different shape than that of a planet (Schneider 1997), though the signal could be confused with limb-darkening effects and would likely be important only for outer gas giants where icy rings can form more easily.

Finally, variations in the ingress timing of inner planets can be used to search for cyclic variations that could betray the presence of moons (Schneider 1997) or — in principle — massive (inner or outer) planets that are nearly coplanar but too misaligned to cause a detectable transit themselves. Transit timing shifts would be caused by the slight orbital motion of the planet around the planet-moon barycenter or that of the star around the system barycenter. (The latter is unobservable for a single-planet system since the star's motion is always phase-locked with the planet.)

3. Principles of Planet Detection via Microlensing

Microlensing occurs when a foreground compact object (e.g., a star) moves between an observer and a luminous background object (e.g., another star). The gravitational field of the foreground lens alters the path of the light from the background source, bending it more severely the closer the ray passes to the lens. This results in an image as seen by a distant observer that is altered both in position and shape from that of the unlensed source. Indeed since light from either side of a lens can now be bent to reach the observer, multiple images are possible (Fig. 10). Since the total flux reaching the observer from these two images is larger than that from the unlensed source alone, the lens (and any planets that may encircle it) betrays its presence not through its own luminous emission, but by its gravitational magnification of the flux of background objects. Einstein (1936) recognized microlensing in principle, but thought that it was undetectable in practice.

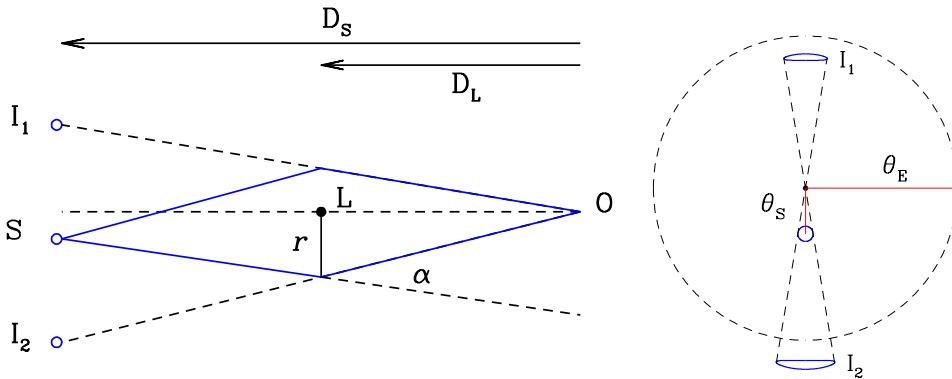


Fig. 10 — **Left:** A compact lens (L) located a distance D_L nearly along the line-of-sight to a background source (S) located at a distance D_S will bend incoming light rays by differing amounts α to create two images (I_1 and I_2) on either side of the line-of-sight. **Right:** An observer O does not see the microlensed source at its true angular sky position θ_S , but rather two images at positions θ_1 and θ_2 .

Ray tracing, together with the use of general relativity to relate the bending angle α with the lens mass distribution, produces a mapping from the source positions (ξ, η) to the image positions (x, y) for a given mass distribution. For “point” masses, the angle α is just given by the mass of the lens M and the distance of closest approach r as:

$$\alpha = \frac{4GM}{c^2 r} = \frac{2R_S}{r} \quad , \quad (13)$$

as long as r is well outside the Schwarzschild radius R_S of the lens. Simple

geometry alone then requires

$$\theta_S D_S = r \frac{D_S}{D_L} - (D_S - D_L) \alpha(r) \quad , \quad (14)$$

which can be rewritten to yield the lens equation

$$\theta_S = \theta - \frac{D_{LS}}{D_S} \alpha(r) \quad , \quad (15)$$

giving the (angular) vector image positions θ for a source at the angular position θ_S as measured from the observer-lens line-of-sight. D_S and D_L are the source and lens distances from the observer, respectively, and $D_{LS} \equiv D_S - D_L$.

For convenience, the characteristic angular size scale is defined as

$$\theta_E \equiv \sqrt{\frac{2R_S D_{LS}}{D_L D_S}} = \sqrt{\frac{4GM D_{LS}}{c^2 D_L D_S}} \quad . \quad (16)$$

Since $r = D_L \theta$, Eq. 15 can now be rewritten to yield a quadratic equation in θ

$$\theta^2 - \theta_S \theta - \theta_E^2 = 0 \quad , \quad (17)$$

with two solutions $\theta_{1,2} = \frac{1}{2} \left(\theta_S \pm \sqrt{4\theta_E^2 + \theta_S^2} \right)$ giving the positions of images I_1 and I_2 . When the source lies directly behind the lens as seen from the observer, $\theta_S = 0$ and the two images merge into a ring of radius θ_E , the so-called ‘‘Einstein ring.’’ For all other source positions, one image will lie inside θ_E and one outside. The flux observed from each image is the integral of the image surface brightness over the solid angle subtended by the (distorted) image. Since the specific intensity of each ray is unchanged in the bending process, so is the surface brightness. The magnification $A_{1,2}$ for each image is then just the ratio of the image area to the source area, and is found formally by evaluating at the image positions the determinant of the Jacobian mapping J that describes the lensing coordinate transformation from image to source plane:

$$A_{1,2} = \frac{1}{|\det J|} \Big|_{\theta=\theta_{1,2}} = \left| \frac{\partial \theta_S}{\partial \theta} \right|_{\theta=\theta_{1,2}}^{-1} \quad , \quad (18)$$

where θ_S and θ are (angular) position vectors for the source and image, respectively.

What is most important for detection of extra-solar planets around lenses is not the position of the images but their magnification. For stellar lenses and typical source and lens distances within the Milky Way, the

typical image separation ($\gtrsim 2\theta_E$) is ~ 1 milliarcsecond, too small to be resolved with current optical telescopes. The observer sees one image with a combined magnification $A \equiv A_1 + A_2$ that can be quite large. In order to distinguish intrinsically bright background sources from fainter ones that appear bright due to microlensing, the observer relies on the characteristic brightening and dimming that occurs as motions within the Galaxy sweep the source (nearly) behind the lens-observer line-of-sight. The unresolved images also sweep across the sky (Fig. 11); their combined brightness reaches its maximum when the source has its closest projected distance to the lens.

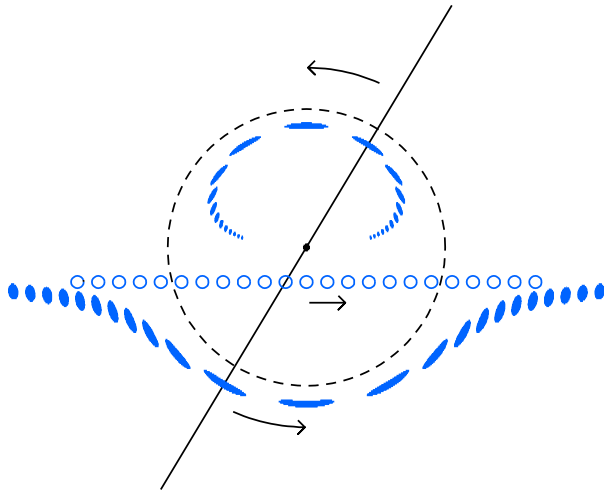


Fig. 11 — As a background source (open circle) moves nearly behind a foreground lens (central dot), the two microimages remain at every moment colinear with the lens and source. (Adapted from Paczyński 1996.)

For a single lens, the combined magnification can be shown from Eqs. 17 and 18 to be:

$$A = \frac{u^2 + 2}{u\sqrt{u^2 + 4}} \quad , \quad (19)$$

where $u \equiv \theta_S/\theta_E$ is the angular source-lens separation in units of the Einstein ring radius. For rectilinear motion, $u(t) = \sqrt{(t - t_0)^2/t_E^2 + u_{min}^2}$, where t_0 is the time at which u is minimum and the magnification is maximum, and $t_E \equiv \theta_E D_L/v_{\perp}$ is the characteristic time scale defined as the time required for the lens to travel a projected distance across the observer-source sightline equal to the Einstein radius r_E . The result is a symmetric light curve that has a magnification of 1.34 as it crosses the Einstein ring radius and a peak amplification that is approximately inversely propor-

tional to the source impact parameter u_{min} . Since the u_{min} are distributed randomly, all of the light curves shown in Fig. 12 are equally probable.

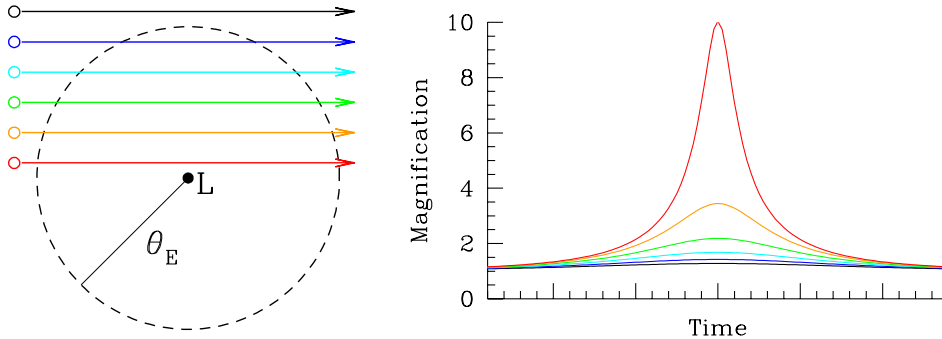


Fig. 12 — **Left:** Equally-probable source trajectories. **Right:** The corresponding single microlens light curves.

Typical event durations $\hat{t} = 2t_E$ for microlensing events detected in the direction of the Galactic Bulge are on the order of a few weeks to a few months, generally matching expectations for stellar lenses distributed in the Galactic disk and bulge.

3.1. MICROLENSING BY BINARY LENSES

Microlensing was proposed as a method to detect compact baryonic dark matter in the Milky Way by Paczyński in 1986. In 1991, Mao and Paczyński suggested that not only dark lenses, but possible dark planets orbiting them may be detected through their microlensing influence on background stars.

The magnification patterns of a single lens are axially symmetric and centered on the lens; the Einstein ring radius, for example, describes the position of the $A \equiv A_1 + A_2 = 1.34$ magnification contour. Binary lens structure destroys this symmetry: the magnification patterns become distorted and are symmetric only upon reflection about the binary axis. Positions in the source plane for which the determinant of the Jacobian (Eq. 18) is zero represent potential source positions for which the magnification is formally infinite. The locus of these positions is called a “caustic.” For a single point-lens, the only such position is the point caustic at $\theta_S = 0$, but the caustics of binary lenses are extended and complicated in shape. In the lens plane, the condition $|\det J| = 0$ defines a locus of points known as the critical curve; when the source crosses a caustic a pair of new images of high amplification appear with image positions θ on the critical curve.

A static lens configuration has a fixed magnification pattern relative to the lens; the observed light curve is one-dimensional cut through this

pattern that depends on the source path. As Fig. 13 illustrates, the exact path of the source trajectory behind a binary lens will determine how much its light curve deviates from the simple symmetric form characterizing a single lens. Due to the finite size of the source, the magnification during a caustic crossing is not infinite, but will be quite large for sources that are small compared to the size of the caustic structure. Several binary-lens light curves have already been observed and characterized (Udalski *et al.* 1994, Alard, Mao & Guibert 1995, Alcock *et al.* 1997, Albrow *et al.* 1998b, Albrow *et al.* 1999).

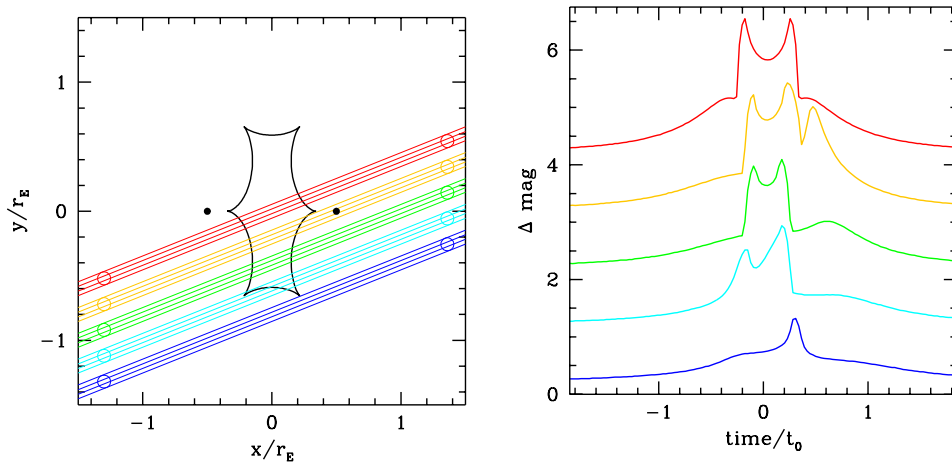


Fig. 13 — **Left:** The caustic (thick closed line) for two equal mass lenses (dots) is shown with several possible source trajectories. Angular distances are scaled to the Einstein ring radius of the combined lens mass. **Right:** The light curves resulting from the source trajectories shown at left; the temporal axis is normalized to the Einstein time t_E for the combined lens. (Adapted from Paczyński 1996.)

A single lens light curve is described by four parameters: the Einstein crossing time t_E , the impact parameter u_{min} , the time of maximum amplification t_0 , and the unlensed flux of the source F_0 . Only the first of these contains information about the lens itself. Three additional parameters are introduced for binary lenses: the projected separation b of the lenses in units of θ_E , the mass ratio q of the two lenses, and the angle ϕ that the source trajectory makes with respect to the binary axis. Given the large number of free parameters and the variety of complicated forms that binary light curves can exhibit, it may seem quite difficult to characterize the binary lens with any degree of certainty on the basis of a single 1-D cut through its magnification pattern. In fact, with good data the fitting procedure is unique enough that the *future* behavior of the complicated light curve — including the timing of future caustic crossings — can be predicted in real

time. This is important since the ability to characterize extra-solar planets via microlensing requires proper determination of the planetary system parameters b and q through modeling of light curve anomalies.

3.2. PLANETARY MICROLENSING

The simplest planetary system is a binary consisting of a stellar lens of mass M_* orbited by a planet of mass m_p at an orbital separation a . The parameter range of interest is therefore $q \equiv M_*/m_p \approx 10^{-3}$ for jovian-mass planets and $q \approx 10^{-5}$ for terrestrial-mass planets. The normalized projected angular separation $b \lesssim a/(\theta_E D_L)$ depends at any moment on the inclination and phase of the planetary orbit. The light curve of a source passing behind a lensing planetary system will depend on the form of the magnification pattern of the lensing system, which is influenced by the size and position of the caustics. How do the magnification patterns vary with b and q ?

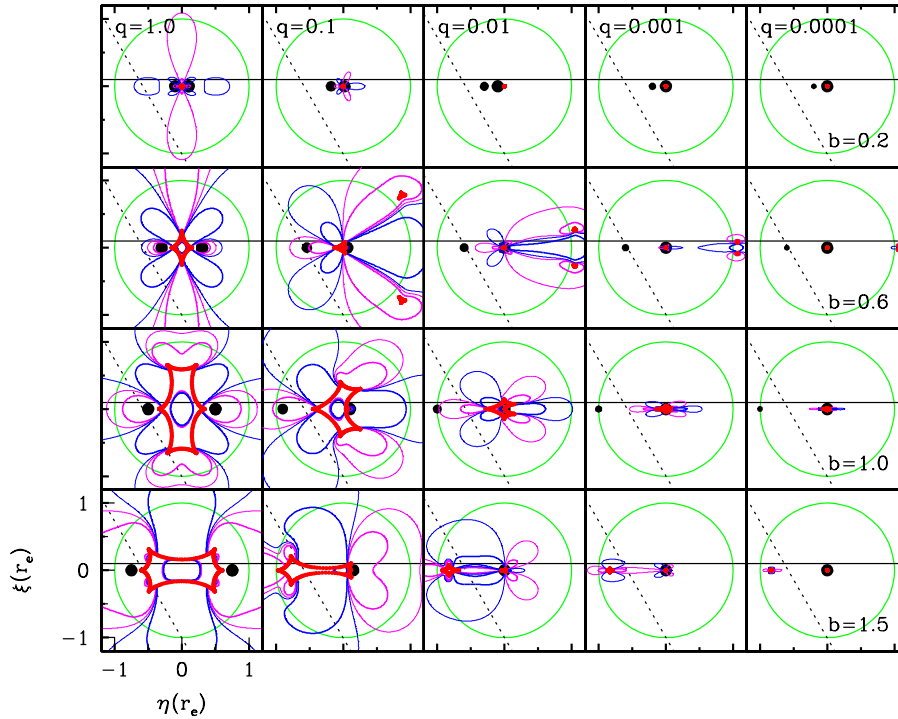


Fig. 14 — Positive (magenta) and negative (blue) 1% and 5% *excess* magnification contours for binary lenses (black dots) of different projected separations b and mass ratios q . Caustics are shown in red. Dimensions are normalized to the Einstein ring radius of combined system (green circle). Dashed and solid lines are two possible source trajectories. (Adapted from Gaudi & Sackett 1998.)

Shown in Fig. 14 is the *excess* magnification pattern of a binary over that of a single lens for different separations b and mass ratios q . The deviations can be positive or negative. High-mass ratio binaries (i.e., q not too much less than 1) are easier to detect since their excess magnification contours cover a larger sky area making it more likely that a source trajectory will cross an “anomalous” region. For a given mass ratio q , the 1% and 5% excess magnification contours also cover more sky when the binary separation is comparable to the Einstein ring radius of the system, i.e., whenever $b \approx 1$.

The symmetric caustic structure centered between equal mass ($q = 1$) binaries becomes elongated along the binary axis for smaller mass ratios, eventually splitting the caustic into a central caustic centered on the primary lens and outer “planetary” caustics. For planetary separations larger than the Einstein ring radius $b > 1$, the planetary caustic is situated on the binary axis between the lens and planet. For $b < 1$, the planetary caustics are two “tips” that are symmetrically positioned above and below the binary axis on the opposite side of the lens from the planet. As the mass ratio decreases, all the caustics shrink in size and the two “tips” approach the binary axis, nearly — but not quite — merging.

3.2.1. The “Lensing Zone”

For the planetary (small q) regime, a source that crosses the central caustic will generate new images near the Einstein ring of the primary lens; a source crossing a planetary caustic will generate new images near the Einstein ring of the planet, i.e., near the position of the planet itself. Planets with separations $0.6 \lesssim b \lesssim 1.6$ create planetary caustics inside the Einstein ring radius of the parent lensing star; this is the region in which the source must be in order to be alerted by the microlensing survey teams. For this reason, planets with projected separations $0.6 \lesssim b \lesssim 1.6$ are said to lie in the “lensing zone.” Since the separation b is normalized to the size of the Einstein ring, the physical size of the lensing zone will depend on the lens mass and on the lens and source distances. Most of the microlensing events in the Milky Way are detected in the direction of the Galactic bulge where, at least for the bright red clump sources, it is reasonable to assume that the sources lie at $D_S \approx 8$ kpc. Table I shows the size of the lensing zone for foreground lenses located in the disk ($D_L = 4$ kpc) and bulge ($D_L = 6$ kpc) for typical stellar masses, assuming that $D_S = 8$ kpc.

One of the reasons that microlensing is such an attractive method to search for extra-solar planets is that the typical lensing zone corresponds to projected separations of a few times the Earth-Sun distance (AU) — a good match to many planets in the Solar System. Planets orbiting at a radius a in a plane inclined by i with respect to the plane of the sky will traverse a range of projected separations $a \cos i / (\theta_E D_L) < b < a / (\theta_E D_L)$,

and can thus be brought into the lensing zone of their primary even if their orbital radius is larger than the values given in Table I.

| | disk lens (4 kpc) | bulge lens (6 kpc) |
|----------------------------|-------------------|--------------------|
| 1.0 M_{\odot} solar-type | 2.4 - 6.4 AU | 2.1 - 5.5 AU |
| 0.3 M_{\odot} dwarf | 1.3 - 3.5 AU | 1.1 - 3.0 AU |

Planets that are seldom or never brought into the lensing zone of their primary can still be detected by microlensing in one of two ways. Either the light curve must be monitored for source positions outside the Einstein ring radius of the primary (i.e., for magnifications $A < 1.34$) in order to have sensitivity to the isolated, outer planetary caustics (DiStefano & Scalzo 1999), or very high amplification events must be monitored in order to sense the deviations that are caused any planet on the central primary caustic (Griest & Safizadeh 1998).

3.2.2. Determining the Planet-Star Mass Ratio and Projected Separation

The generation of caustic structure and the anomalous magnification pattern associated with it makes planetary masses orbiting stellar lenses easier to detect than isolated lensing planets. Even so, most planetary light curves will be anomalous because the source passed near, but not across a caustic (Fig. 15). How is the projected planet-star separation b and the planet-star

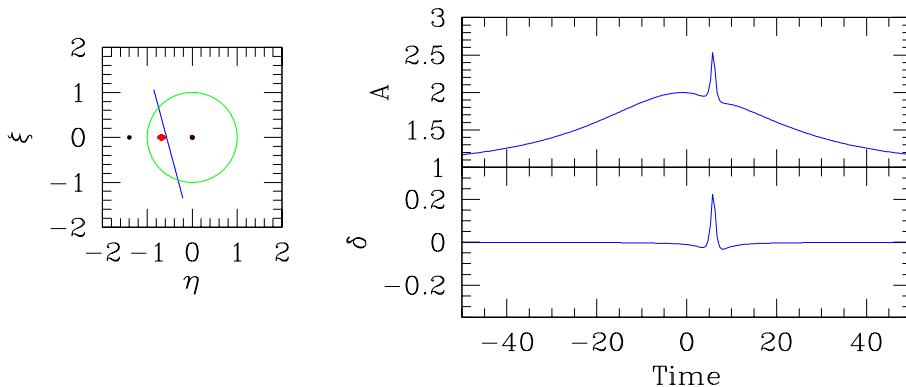


Fig. 15 — **Left:** A background point source travels along the (blue) trajectory that just misses the (red) caustic structure caused by a “Jupiter” with mass ratio $q = 0.001$ located at 1.3 Einstein ring radii (several AU) from its parent stellar lens. **Right:** The resulting light curve is shown in the top panel; the excess magnification δ associated with the planetary anomaly is shown in the bottom panel; time scale is in days.

mass ratio $q = m_p/M_*$ extracted from a planetary anomaly atop an otherwise normal microlensing light curve? In practice, the morphology of planetary light curve anomalies is quite complex, and detailed modeling of the excess magnification pattern (the anomalous change in the pattern due to the planet) is required, but the general principles can be easily understood.

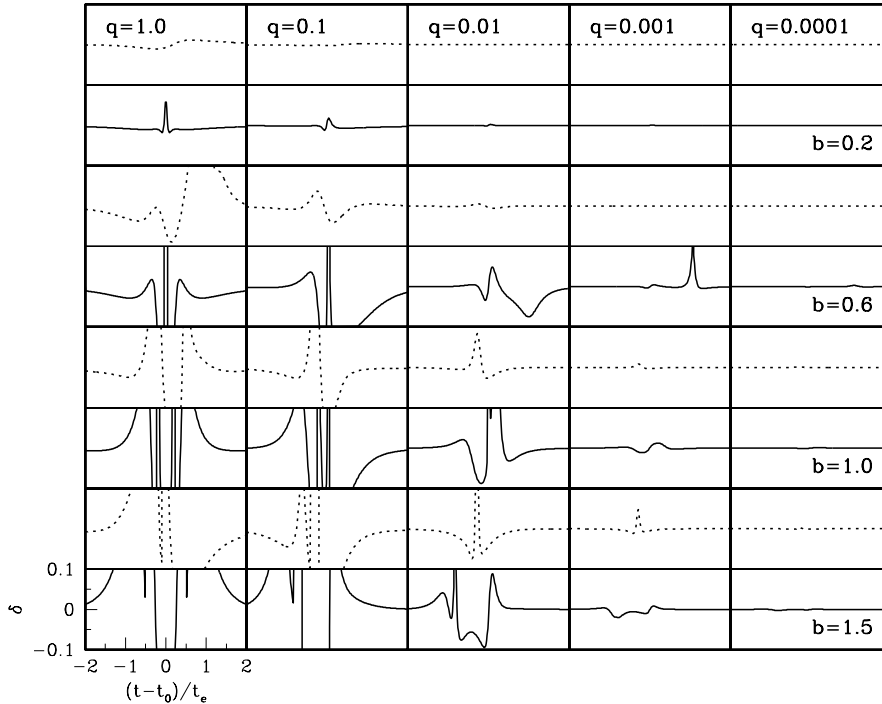


Fig. 16 — Excess magnifications δ for the (solid and dotted) trajectories of Fig. 14 are shown for (the same) range of planetary mass ratios and projected separations. “Super-jupiters” with $q \sim 0.01$ should create detectable anomalies for a significant fraction of source trajectories in high quality light curves. (Adapted from Gaudi & Sackett 1998.)

Since the planet and parent star lenses are at the same distance D_L and travel across the line of sight with the same velocity v_\perp (ignoring the planet’s orbital motion), Eq. 16 shows that the mass ratio q is equal to the square of the ratio of the Einstein ring radii $(\theta_p/\theta_E)^2$. Observationally this can be estimated very roughly by the square of the ratio of the planetary anomaly duration to the primary event duration, $(t_p/t_E)^2$. The time difference between the primary and anomalous peaks (normalized to the Einstein time) gives an indication of the placement of the caustic structure within the Einstein ring and thus the position of the planet relative to the primary lens, b . The amplitude of the anomaly $\delta \equiv (A - A_0)/A_0$, where A_0

is the unperturbed amplitude, indicates the closest approach to the caustic structure and, together with the temporal placement of the anomaly, yields the source trajectory angle through the magnification pattern.

Since the magnification pattern associated with planetary caustics for $b > 1$ and $b < 1$ planets is qualitatively different, detailed dense monitoring should resolve any ambiguity in the planetary position. Light curve anomalies associated with $b > 1$ planets, like the one in Fig. 15, will have relatively large central peaks in δ surrounded by shallow valleys; $b < 1$ anomalies will generally have more rapidly varying alterations of positive and negative excess magnification, though individual exceptions can certainly be found.

From the shape of light curve anomalies alone, the mass of the planet is determined as a fraction of the primary lens mass; its instantaneous projected separation is determined as a fraction of the primary Einstein radius. Reasonable assumptions about the kinematics, distribution, and masses of the primary stellar lenses, together with measurements of the primary event duration $2t_E$ and fraction of blended light from the lens should allow r_E and M_* to be determined to within a factor $\sim 3 - 5$. Detailed measurements of the planetary anomaly would then yield the absolute projected separation and planetary mass to about the same precision.

3.2.3. Durations and Amplitudes of Planetary Anomalies

It is clear from Figs. 14 and 16 that, depending on the source trajectory, a range of anomaly durations t_p and amplitudes δ are possible for a planetary system of given q and b (see also Wambsganss 1977). Nevertheless, rough scaling relations can be developed to estimate the time scales and amplitudes that will determine the photometric sampling rate and precision required for reasonable detection efficiencies to microlensing planetary systems.

For small mass ratios q , the region of excess magnification associated with the planetary caustic is a long, roughly linear region with a width approximately equal to the Einstein ring of the planet, θ_p , and a length along the planet-lens axis several times larger. Since $\theta_p = \sqrt{q} \theta_E$, both the time scale of the duration and the cross section presented to a (small) source vary linearly with θ_p/θ_E and thus with \sqrt{q} . Assuming a typical $t_E = 20$ days, the duration of the planetary anomaly is given roughly by the time to cross the planetary Einstein diameter, $2\theta_p$,

$$\text{planet anomaly duration} = 2t_p \approx 1.7 \text{ hrs } (m/M_\oplus)^{1/2} (M/M_\odot)^{-1/2}. \quad (20)$$

Caustic crossings can occur for any planetary mass ratio and should be easy to detect as long as the temporal sampling is well matched to the time scales above. Most anomalies, however, will be more gentle perturbations

associated with crossing lower amplitude excess magnification contours. At the most favorable projected lens-planet separation of $b = 1.3$, and the most ideal lens location (halfway to the Galactic Center), well-sampled observations able to detect 5% perturbations in the light curve would have planet sensitivities given roughly by (Gould & Loeb 1992):

$$\text{ideal detection sensitivity} \approx 1\% (m/M_{\oplus})^{1/2} (M/M_{\odot})^{-1/2} \quad (21)$$

This ideal sensitivity is relevant only for planets at $b = 1.3$; at the edges of the lensing zone the probabilities are about halved. Detection with this sensitivity requires photometry at the 1% level, well-sampled over the duration of the planetary event.

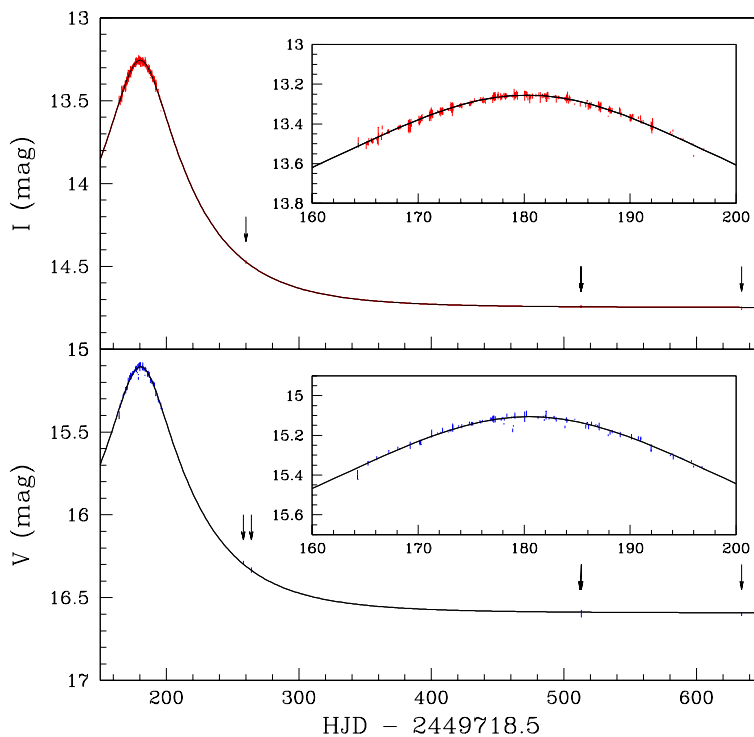


Fig. 17 — PLANET collaboration monitoring of MACHO-BLG-95-13 in the I (upper) and V (lower) bands. Insets show a zoom around the peak of the event; arrows indicate points taken many months to more than a year later. Vertical scale is magnitudes; horizontal scale is days (Albrow *et al.* 1998a).

Can such photometric precision and temporal sampling be obtained in the crowded fields of the Galactic bulge where nearly all microlensing events are discovered? Fig. 17 shows observations of one bright microlensing event monitored by the PLANET collaboration during its month-long pilot

season in 1995 (Albrow *et al.* 1998a). The residuals from the single point-lens/point source light curve are less than 1% for this event, and the typical sampling rate is on the order of once every 1-2 hours, even accounting for unavoidable longitudinal and weather gaps.

A true calculation of detection probabilities must integrate over the projected orbital separations and the distribution of lenses along the line of sight, must take into account the actual distribution of source trajectories probed by a particular set of observations, and the effect of uneven temporal sampling and photometric precision (Gaudi & Sackett 1998). In the following section we discuss the additional complication of finite source effects that is encountered for very small mass planets for which the size of the planetary Einstein ring is comparable to or smaller than the source size, $\theta_p \lesssim \theta_*$.

3.3. OBSERVATIONAL REWARDS AND CHALLENGES

What can be learned by observing a planetary anomaly in a microlensing light curve? The duration, temporal placement relative to the event peak, and relative amplitude of the anomaly can be used to determine the mass ratio q of the planetary companion to the primary (presumably stellar) lens and their projected angular separation b in units of the Einstein ring radius θ_E . Since in general the lens will be far too distant to type spectrally against the bright background source (except possibly with very large apertures, see Mao, Reetz & Lennon 1998), the absolute mass and separation must be determined statistically by fitting the properties of an ensemble of events with reasonable Galactic assumptions. Measurements of other sorts of microlensing anomalies associated with source resolution, observer motion, or lens blending can produce additional constraints on the lens properties and thus on the absolute planetary characteristics.

Except for very large a planets orbiting in nearly face-on ($i \approx 0$) orbits, cooperative lensing effects between the lens and companion boost the detectability of lensing planets over that expected for planets in isolation. Since current detection and monitoring schemes focus on those events with an essentially random distribution of impact parameters u_{min} for $u_{min} < 1$, the anomaly sensitivity is primarily restricted to planets in the “lensing zone” with projected separations of 0.6 — 1.6 times the Einstein ring radii of the primary lens. For typical distributions of lens masses, and lens and source distances, this translates into the highest probabilities for planets with instantaneous orbital separations *projected onto the sky plane* of $a_p \approx 5$ AU, with a zone of reduced detectability extending to higher a_p . Since the efficiency of planetary detection in these zones is likely to be a few or a few tens of percent (Eq. 21), many microlensing events must be

monitored with $\sim 1\%$ photometry on the \sim hourly time scales (Eq. 20) to achieve statistically meaningful constraints on the number planets in the Milky Way, and their distribution in mass and orbital radius.

What limits the photometric precision and temporal sampling? Round-the-clock monitoring of events, necessary for maximum sensitivity to the 1 – 2 day durations of Jupiter-mass anomalies requires telescopes scattered in geographical longitude, at the South Pole, or in space. Temporal sampling is limited by the number of events monitored at any given time, their brightness, and the desired level of photometric precision. Higher signal-to-noise can generally be obtained for brighter stars in less exposure time, but ultimately, in the crowded fields that typify any microlensing experiment, photometric precision is limited by confusion from neighboring sources, not photon statistics. Pushing below $\sim 1\%$ relative photometry with current techniques has proven very difficult in crowded fields.

If an anomaly is detected, it must be distinguished from other intrinsic effects that could be confused with a lensing planet. Stellar pulsation on daily to sub-daily time scales in giant and sub-giant bulge stars is unlikely, but this and any form of regular variability would easily be recognized as periodic (i.e., non-microlensing) with the dense and precise sampling that is required in microlensing monitoring designed to detect planets. Star-spot activity may be non-negligible in giants, but will have a time scale characteristic of the rotation period of giants, and thus much longer than typical planetary anomalies. In faint dwarf stars spotting activity produces flux changes below the photometric precision of current experiments. Flare activity should not be significant for giants and is expected to be chromatic, whereas the microlensing signal will always be achromatic (except in the case of source resolution by exceedingly low-mass planets).

Blending (complete photometric confusion) by random, unrelated stars along the line-of-sight can dilute the apparent amplitude of the primary lensing event. This will have some effect on the detection efficiencies, but most significantly — with data of insufficient sampling and photometric precision — will lead to underestimates for the time scale t_E and impact parameter u_{min} of the primary event, and thus also to mis-estimates of the planetary mass ratio q and projected separation b .

3.3.1. *Pushing the Limits: Earth-mass and Multiple Planets*

Planets with very small mass ratio will have caustic structure smaller than the angular size of typical bulge giants. The ensuing dilution of the anomaly by finite source effects will present a large, but perhaps not insurmountable, challenge to pushing the microlensing planet detection technique into the regime of terrestrial-mass planets (Peale 1997, Sackett 1997).

Near small-mass planetary caustics, different parts of the source simul-

taneously cross regions of significantly different excess magnification; an integration over source area is required in order to derive the total magnification. The severity of the effect can be seen in Fig. 18. Earth-mass caustic crossings against even the smaller-radii bulge sources will present a challenge to current photometry in crowded fields, which is generally limited by seeing to stars above the turn-off mass.

The most numerous, bright microlensing sources in the bulge are clump giants with radii about 13 times that of the Sun ($13 R_\odot$), and thus angular radii of 7.6 microarcseconds (μas) at 8 kpc. Since a Jupiter-mass planet with $m_p = 10^{-3} M_\odot$ has an angular Einstein ring radius of $32 \mu\text{as}$ at 4 kpc and $19 \mu\text{as}$ at 6 kpc, its caustic structure is large compared to the size of the source. An Earth-mass planet with $m = 3 \times 10^{-6} M_\odot$, on the other hand, has an angular Einstein ring radius of $1.7 \mu\text{as}$ at 4 kpc and $1 \mu\text{as}$ at 6 kpc, and will thus suffer slight finite source effects even against turn-off stars ($1.7 \mu\text{as}$), though the effect will be greatly reduced compared to giant sources (Bennett & Rhie 1996).

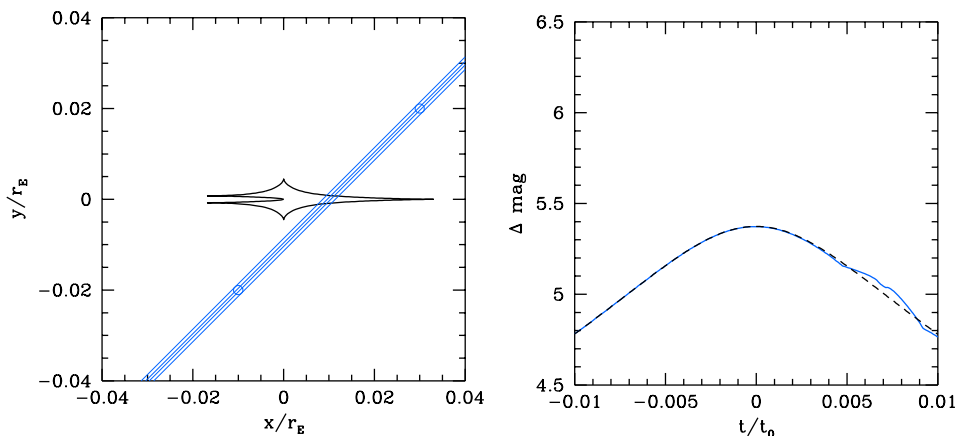


Fig. 18 — **Left:** A source of angular size $\theta_* = 0.001 \theta_E$, typical of turn-off stars in the bulge, crosses the central caustic caused by a terrestrial-mass planet with mass ratio $q = 10^{-5}$. **Right:** Due to source resolution effects, the resulting anomaly differs from single-lens microlensing only at the $\sim 1\% - 3\%$ level. Note the expanded spatial and temporal scales. (Adapted from Paczyński 1996.)

For extreme source resolution, in which the entire planetary caustic lies inside the projected source radius, the *excess fractional* magnification associated with the planetary anomaly scales with the square of the ratio of the planetary Einstein ring radius to the angular source size, $\delta \propto (\theta_p/\theta_*)^2$. On the other hand, source-resolved small q anomalies will have longer durations than implied by Eq. 20, since the characteristic time scale is the time to cross the source θ_* (not θ_p). Furthermore, the cross section for magnifi-

cation at a given threshold now roughly scales with θ_*/θ_E (not θ_p/θ_E), and is thus approximately independent of planetary mass.

Because the anomaly amplitude is suppressed by source resolution, unless the photometry is excellent and continuous, small-mass planetary caustic crossings can be confused with large impact parameter large-mass planetary anomalies. This degeneracy can be removed by performing multi-band observations (Gaudi & Gould 1997): large impact parameter events will be achromatic, but sources resolved by small-mass caustics will have a chromatic signal due to source limb-darkening that is similar to (but of opposite sign from) that expected for planetary transits (§2.3.1). Source limb-darkening and chromaticity have now been observed during a caustic crossing of a stellar binary (Albrow *et al.* 1998b).

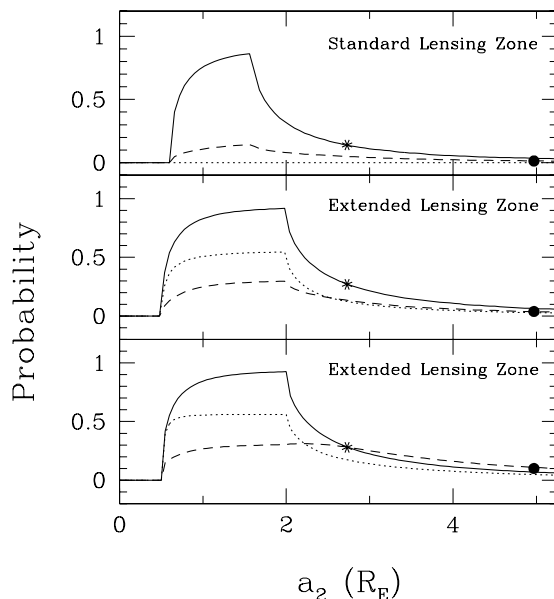


Fig. 19 — **Top:** Probability that two planets with true orbital radii a_1 and a_2 (in units of the Einstein ring r_E) simultaneously have projected separations, b_1 and b_2 , in the standard “lensing zone,” defined as $0.6 < b < 1.6$. The probability is shown as function of a_2 , for fixed $a_1 = 1.5$ (solid), $a_1 = 0.6$ (dotted) and $a_1 = 2.7$ (dashed). The probability for two planets with orbital radii of Jupiter and Saturn around solar-mass primary (star) and a $0.3M_\odot$ primary (dot) are shown. **Middle:** Same, but for the extended “lensing zone,” $0.5 < b < 2.0$. **Bottom:** The conditional probability that both b_1 and b_2 lie in the extended “lensing zone,” given that either b_1 or b_2 satisfies this criterion. (Gaudi, Naber & Sackett 1998.)

Finally, since all planetary lenses create a central caustic, low-impact parameter (high magnification) microlensing events that project the source close to the central caustic are especially efficient in producing detectable

planetary anomalies (Griest & Safizadeh 1998). For the same reason, however, the central caustic is affected by *all* planets in the system, and so — if possible degeneracies due to the increased caustic complexity can be removed — rare, low impact parameter events offer a promising way of simultaneously detecting multiple planets brought into or near the lensing zone by their orbital motion around the primary lens (Gaudi, Naber & Sackett 1998). As Fig. 19 demonstrates, the statistical probabilities are large that a Jupiter or 47UMa orbiting a solar-mass star (solid and dotted lines, respectively) will instantaneously share the lensing zone with other planets of orbital radii of several AU. However, the light curves resulting from crossing a multiple-planet central caustic may be difficult to interpret since the caustic structure is so complicated (Fig. 20).

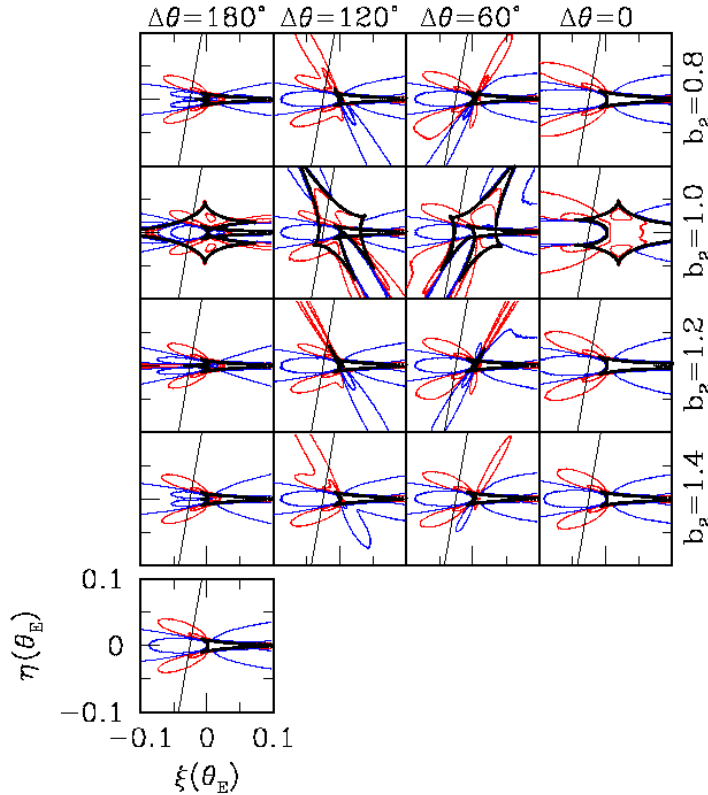


Fig. 20 — Contours of 5% and 20% fractional deviation δ , as a function of source position in units of the θ_E . The parameters of planet 1 are held fixed at $q_1 = 0.003$, $b_1 = 1.2$; the projected separation b_2 and the angle between the axes, $\Delta\theta$, are varied for a second planet with $q_2 = 0.001$. Only planet 1 is present in the bottom offset panel. Positive (red), negative (blue) and caustic ($\delta = \infty$, thick line) contours are shown. (Gaudi, Naber & Sackett 1998.)

4. Photometric Mapping of Unseen Planetary Systems: Matching the Tool to the Task

Both the transit and microlensing techniques use frequent, high-precision monitoring of many stars to discover the presence of the unseen extra-solar planets. The transit method monitors the light from the parent star in search of occultation by an unseen planet; the microlensing technique monitors light from an unrelated background source in search of lensing by an unseen planet orbiting an unseen parent star. Indeed, microlensing is the only extra-solar planetary search technique that requires *no photons from either the planet or the parent star* and for this reason is the method most sensitive to the distant planetary systems in our Galaxy.

The two techniques are complementary, both in terms of the information that they provide about discovered systems, and in terms of the range of planetary system parameters to which they are most sensitive. Multiple transit measurements of the same planet will yield its planetary radius R_p and orbital radius a . Characterization of a microlensing planetary anomaly gives the mass ratio $q \equiv m_p/M_*$ of the planet to lensing star and their projected separation b at the time of the anomaly in units of θ_E .

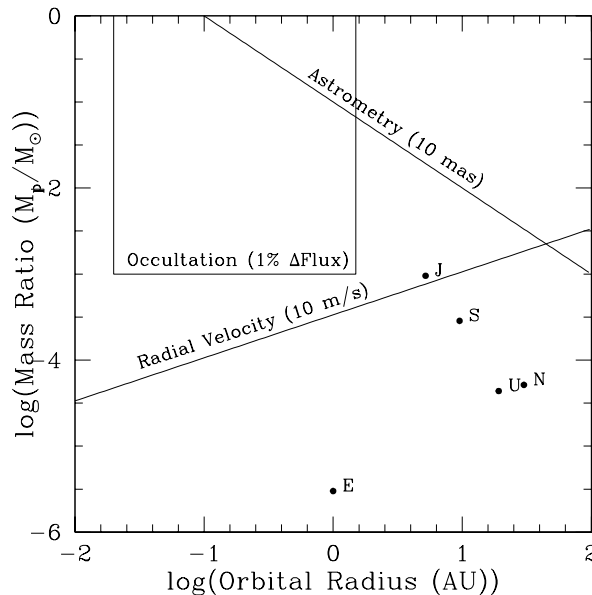


Fig. 21 — Current detection thresholds for long-running programs that rely on planet orbital motion, shown as a function of planetary mass ratio and orbital radius. The occultation threshold must be multiplied by the appropriate geometric probability of a transit to derive detection efficiencies. Selected Solar System planets are shown.

Current ground-based photometry is sensitive to jovian-size occultations; space-based missions may extend this into the terrestrial regime. The transit method is sensitive to planets with small a because they create a detectable transit over a wider range of inclinations of their orbital planes, and because they transit more often within a typical 5-year experiment. These constraints limit the range of orbital radii to about $0.02 \lesssim a \lesssim 1.5$ AU for jovian-size planets. If improvements in photometric precision would allow the detection of Earth-size planetary transits, this range would still be possible, but would suffer from noise due to star spot activity on time scales that could be confused with transits by small-mass planets with $a \lesssim 0.3$ AU.

Since the planets in our solar system fall roughly on the same $\log m_p$ - $\log R_p$ relationship, it is reasonable to assume that jovian-size planets may also have jovian masses. This assumption was used to place the current transit detection capability on the same plot (Fig. 21) with the current detection thresholds for radial velocity and astrometric techniques. All three of these techniques require long-term projects to detect long-period (large a) planets since the measurements of velocity, position, or flux must be collected over at least one full orbital period. The occultation threshold must be convolved with the geometric transit probability to derive efficiencies *per observed star*.

Photometric precision in crowded fields together with source resolution effects limit current microlensing planet searches to Neptune masses and above. The actual efficiency with which a given planetary system can be detected depends on its mass ratio and projected orbital separation. Fig. 22 shows estimates of microlensing detection efficiency contours for planets of a given mass ratio and true orbital separation (in units of the Einstein radius). The contours are based on the work of Gaudi & Gould (1997) for high-mass ratios, Gould & Loeb (1992) and Gaudi & Sackett (1998) for intermediate mass ratios, and Bennett & Rhie (1996) for small ratios. Integrations have been performed over the unknown but presumably randomly oriented inclinations and orbital phases. Although planets with a in the lensing zone and orbiting in the sky plane are the easiest to detect, a tail of sensitivity extends to larger a as well because inclination effects will bring large- a planets into the projected lensing zone for some phases of their orbits. The efficiencies assume $\approx 1\%$ photometry well-sampled over the post-alert part of the microlensing light curve.

Examination of Fig. 22 makes it clear that different indirect planetary search techniques will be sensitive to different portions of the $\log m_p$ - $\log a$ domain. Current ground-based capabilities favor the radial velocity method for short-period ($a \lesssim 3$ AU) planets (see also Queloz, this proceedings). The occultation method will help populate the short-period part of the diagram, and if the programs are carried into space, will begin to probe

the regime of terrestrial-sized planets in terrestrial environments. Ground-based astrometry is favored for very long-period ($a \gtrsim 40$ AU) planets, although the time scales for detection and confirmation are then on the order of decades. Space-based astrometry promises to make this method substantially more efficient, perhaps by a factor of 100 (see also Colavita, this proceedings). Microlensing is the only technique capable of detecting in the near term substantial numbers of intermediate-period ($3 \lesssim a \lesssim 12$ AU) planets. Somewhat longer period planets may also be discovered by microlensing survey projects as independent “repeating” events in which the primary lens and distant planet act as independent lenses (DiStefano & Scalzo 1999). Very short-period planets interior to 0.1 AU may be detectable using the light echo technique (Bromley 1992, Seager & Sasselov 1998, Charbonneau, Jhu & Noyes 1998), at least for parent stars with substantial flare activity, such as late M dwarfs.

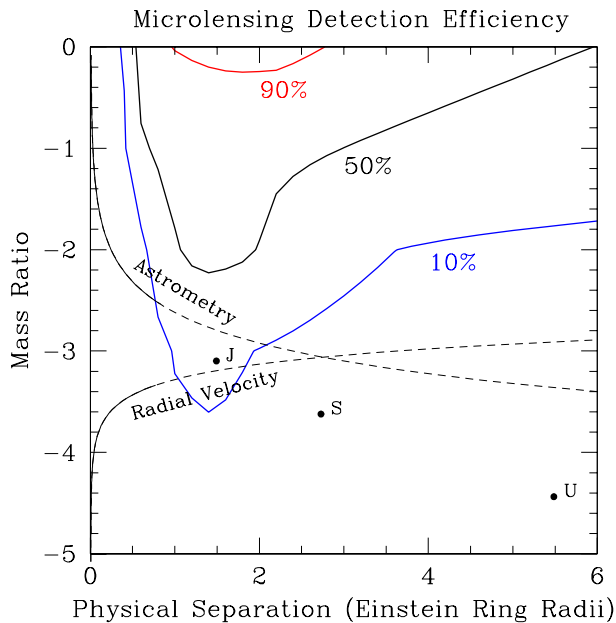


Fig. 22 — Estimated detection efficiency contours for microlensing planet searches as a function of the logarithm of the planetary mass ratio $q \equiv m_p/M_*$ and the true orbital separation a in units of the Einstein ring radius. Efficiencies have been integrated over the phase and inclination of the orbits, under the assumption that they are circular. To make comparisons with other techniques, the Einstein ring radius is taken to be 3.5 AU. Solid lines indicate what can be achieved in an observational program of 5-years duration or less. Note that the vertical scale remains logarithmic, but the horizontal scale is now linear.

The techniques are complementary in another sense as well. Those that rely on light from the parent star will be limited to nearby planetary systems, but will benefit from the ability to do later follow-up studies, including spectroscopy and interferometry. Microlensing, on the other hand, will see the evidence of a given planetary system only once, but can probe planetary frequency in distant parts of the Milky Way, and can collect statistics over a wide range of orbital separations in a relatively short time.

TABLE II. Comparison of Current Ground-Based Capabilities

| | OCCULTATION | MICROLENSING |
|---|----------------------|--|
| Parameters Determined | R_p, a, i | $q \equiv m_p/M_*$, $b \equiv a_p/R_E$ |
| Photometric Precision of | 0.1% | 1% |
| Limits R_p or m_p to | Neptune | Neptune |
| Orbital Radius Sensitivity | $\sim 0.02 - 1.5$ AU | $\sim 1 - 12$ AU |
| Typical Distance of Systems | < 1 kpc | $4 - 7$ kpc |
| Number of Stars to be Monitored | few 10^3 | few 10^2 |
| for Meaningful Jovian Sensitivity at | $\lesssim 1$ AU | ~ 5 AU |
| <i>In Principle Possible to Detect:</i> | | |
| Multiple Planets | yes | yes |
| Planets around Binary Parent Stars | yes | yes |
| Earth-mass Planets in Future | yes (space) | yes |

4.1. TOWARD THE FUTURE

The field of extra-solar planets is evolving rapidly. The number of groups conducting transit and microlensing planet searches, planning future programs, and providing theoretical support is growing at an ever-increasing rate. For that reason, this series of lectures has centered on the principles of the techniques rather than reviewing the current players. In order to help the reader keep pace with this accelerating activity, however, a list of relevant Internet Resources with links to occultation and microlensing planet search groups is provided at the end of this section. What can we expect in the next decade from these research teams?

Several ground-based transit searches are already underway (Villanova University, TEP, WASP, Vulcan, and EXPORT). Some focus on high-quality photometry of known eclipsing binaries. This is likely to increase

the probability of transits — if planets exist in such binary systems. Two transit-search teams recently issued (apparently contradictory) claims for a possible planet detection in the eclipsing M-dwarf system known as CM Draconis (IAU circulars 6864 and 6875, see also Deeg *et al.* 1998), but no clear, undisputed planetary signal has been seen. One class of planets known to exist in reasonable numbers and also relatively easy to detect via occultation is the “hot jupiter;” the planet in 51 Peg is a prototype of this class. If such a planet is the size of Jupiter, its orbital plane would have a $\sim 10\%$ chance of being sufficiently inclined to produce a detectable eclipse of a solar-type parent as seen from Earth. An aggressive ground-based program should be able to detect large numbers of such planets in the next decade — planets that could be studied with the radial velocity technique thereby yielding both planetary mass and radius. Space-based missions (COROT and KEPLER) planned for launch within this decade should have the sensitivity to detect transits from terrestrial-mass objects, but in order to detect Earth-like planets in Earth-like environments (i.e., orbiting solar-type stars at 1 AU) they will need long mission times.

Microlensing planet searches are being conducted or aided by international collaborations (PLANET, GMAN, MPS, MOA, and EXPORT) that intensely monitor the events discovered by microlensing search teams (EROS, MACHO, OGLE, and MOA). MACHO and OGLE electronically alert on-going microlensing in the direction of the Galactic Bulge on a regular basis: at given time during the bulge observing season several events are in progress and available for monitoring. Both the PLANET and GMAN collaborations have issued real-time secondary alerts of anomalous behavior (including binary lenses, source resolution, “lensing parallax”), but to date no clear detection of a lensing planet has been announced. Especially if caustics are crossed, it may be possible to obtain additional information on microlensing planets from the sky motion of the caustics during the event that is induced by planetary motion (Dominik 1998). The number of high-quality microlensing light curves monitored by the PLANET collaboration is already beginning to approach that required for reasonable jovian detection sensitivities (Albrow *et al.* 1998a), so meaningful results on Jupiter look-alikes can be expected within the next few years.

As more telescopes, more telescope time, and wider-field detectors are dedicated to dense, precise photometric monitoring capable of detecting planetary transits and planetary microlensing, we can feel certain that — if jovian planets with orbital radii less than ~ 6 AU exist in sufficient numbers — they will be detected in the next few years by these techniques.

ACKNOWLEDGMENTS

I am grateful to NATO for financial support and to the Institute's efficient and gracious scientific organizers, Danielle Alloin and (the sorely missed) Jean-Marie Mariotti, for a productive and pleasant school. It is also a pleasure to thank B. Scott Gaudi for assistance in the preparation of some of the figures in the microlensing section and for permission to show the results of our work before publication.

INTERNET RESOURCES

General Extra-Solar Planet News:

Extrasolar Planets Encyclopedia (maintained by J. Schneider):
<http://www.obspm.fr/departement/darc/planets/encycl.html>
 and the mirror site in the U.S.A.:
<http://cfa-www.harvard.edu/planets/>

Occultation:

EXPORT: <http://pollux.ft.uam.es/export/>
 TEP: <http://www.iac.es/proyect/tep/tephome.html>
 Villanova University: <http://www.phy.vill.edu/astro/index.htm>
 VULCAN: <http://www.iac.es/proyect/tep/tephome.html>
 WASP: <http://www.psi.edu/esquerdo/wasp/wasp.html>

Microlensing:

EROS: <http://www.lal.in2p3.fr/EROS>
 MACHO: <http://wwwmacho.anu.macho.edu>
 MACHO Alert Page: <http://darkstar.astro.washington.edu>
 OGLE: <http://www.astro.uw.edu.pl/~ftp/ogle>
 MOA: <http://www.phys.vuw.ac.nz/dept/projects/moa/index.html>
 MPS: <http://bustard.phys.nd.edu/MPS/>
 PLANET: <http://www.astro.rug.nl/~planet>

References

1. Alard, C., Mao, S. & Guibert, J. 1995, *Astron. Astrophysics*, 300, L17
2. Albrow et al. 1998a, *Astrophys. J.*, 509, 000, astro-ph/9807299
3. Albrow et al. 1998b, *Astrophys. J.*, in preparation
4. Albrow et al. 1999, *Astrophys. J.*, 512, 000, astro-ph/9807086
5. Alcock, C. *et al.* 1997, *Astrophys. J.*, 479, 119
6. Bennett, D. & Rhie, S. H. 1996, *Astrophys. J.*, 472, 660
7. Borucki, W.J. & Summers, A. L. 1984, *Icarus*, 58, 121
8. Borucki, W.J., Scargle, J.D., Hudson, H.S. 1985, *Astrophys. J.*, 291, 852
9. Bromley, B.C. 1992, *Proc. Astron. Soc. Pacific*, 104, 1049
10. Butler, P., & Marcy, G. 1996, *Astrophys. J.*, 464, L15
11. Charbonneau, D., Jha, S. & Noyes, R.W. 1998, *Astrophys. J.*, 507, L153
12. Colavita M. 1998, this proceedings.
13. Deeg, H.J. *et al.* 1998, *Astron. Astrophysics*, 338, 479
14. Dominik, M. 1998, *Astron. Astrophysics*, 329, 361
15. Di Stefano, R., & Scalzo, R. 1999, *Astrophys. J.*, 512, 000, astro-ph/9810147
16. Einstein, A. 1936, *Science*, 84, 506
17. Gaudi, B. S., & Gould, A. 1997, *Astrophys. J.*, 486, 85
18. Gaudi, B.S., Naber, R.M. & Sackett, P.D. 1998, *Astrophys. J.*, 502, L33-37
19. Gaudi, B.S. & Sackett, P.D. 1998, in preparation
20. Hale, A., & Doyle, L.R. 1994, *Astro. and Space Sci.*, 212, 335
21. Henry, G.W., Baliunas, S.L., Donahue, R.A., Soon, W.H. & Saar, S.H. 1997, *Astrophys. J.*, 474, 503
22. Gould, A., & Loeb, A. 1992, *Astrophys. J.*, 396, 104
23. Griest, K., & Safizadeh, N. 1998, *Astrophys. J.*, 500, 37
24. Laurent, E. & Schneider J. 1998, this proceedings.
25. Mao, S., Reetz, J. & Lennon, D.J. 1998, *Astron. Astrophysics*, 338, 56
26. Mao, S., & Paczyński, B. 1991, *Astrophys. J.*, 374, 37
27. Mayor, M., & Queloz, D. 1995, *Nature*, 378, 355
28. Paczyński, B. 1986, *Astrophys. J.*, 304, 1
29. Paczyński, B. 1996, *Ann. Rev. Astron. & Astrophysics*, 34, 419
30. Queloz, D. 1998, this proceedings.
31. Rosenblatt, F. 1971, *Icarus*, 14, 71
32. Peale, S. J. 1997, *Icarus*, 127, 269
33. Sackett, P.D. 1997, Final Report of the *ESO Working Group on the Detection of Extrasolar Planets*, astro-ph/9709269
34. Schneider, J. 1994, *Planet. Space Sci.*, 42, 539
35. Schneider, J. 1997, Final Report of the *ESO Working Group on the Detection of Extrasolar Planets*
36. Seager, S. & Sasselov, D., 1998, *Astrophys. J.*, 502, L157
37. Sturve, O. 1952, *The Observatory*, 72, 199
38. Udalski, A. *et al.* 1994, *Astrophys. J.*, 436, L103
39. Wambsganss, J. 1997, *Mon. Not. Royal Astron. Soc.*, 284, 172